A NEW DENSITY VARIANCE–MACH NUMBER RELATION FOR SUBSONIC AND SUPERSONIC ISOTHERMAL TURBULENCE

L. KONSTANDIN[1], P. GIRICHIDIS[1,2,3], C. FEDERRATH[1,4], AND R. S. KLESSEN[1]

[1] Zentrum für Astronomie, Institut für Theoretische Astrophysik, Universität Heidelberg, Albert-Ueberle-Str.2,
D-69120 Heidelberg, Germany; konstandin@stud.uni-heidelberg.de
[2] Max Planck Institut für Astrophysik, Karl-Schwarzschild-Str. 1, D-85741 Garching, Germany
[3] Hamburger Sternwarte, Gojenbergsweg 112, D-21029 Hamburg, Germany
[4] Monash Centre for Astrophysics (MoCA), School of Mathematical Sciences, Monash University, Vic. 3800, Australia

ABSTRACT

The probability density function of the gas density in subsonic and supersonic, isothermal, driven turbulence is analyzed using a systematic set of hydrodynamical grid simulations with resolutions of up to 1024^3 cells. We perform a series of numerical experiments with root-mean-square (rms) Mach number $\mathcal{M}$ ranging from the nearly incompressible, subsonic ($\mathcal{M} = 0.1$) to the highly compressible, supersonic ($\mathcal{M} = 15$) regime. We study the influence of two extreme cases for the driving mechanism by applying a purely solenoidal (divergence-free) and a purely compressive (curl-free) forcing field to drive the turbulence. We find that our measurements fit the linear relation between the rms Mach number and the standard deviation (std. dev.) of the density distribution in a wide range of Mach numbers, where the proportionality constant depends on the type of forcing. In addition, we propose a new linear relation between the std. dev. of the density distribution σ_ρ and that of the velocity in compressible modes, i.e., the compressible component of the rms Mach number, $\mathcal{M}_{\mathrm{comp}}$. In this relation the influence of the forcing is significantly reduced, suggesting a linear relation between σ_ρ and $\mathcal{M}_{\mathrm{comp}}$, independent of the forcing, and ranging from the subsonic to the supersonic regime.

Key words: hydrodynamics – ISM: kinematics and dynamics – ISM: structure – methods: numerical – shock waves – turbulence

Online-only material: color figures

1. INTRODUCTION

Understanding the intricate interplay between interstellar turbulence and self-gravity is one of the key problems in star formation theory. The supersonic turbulent velocity field is likely responsible for the complex and filamentary density structures observed in molecular clouds. It creates dense regions that can become gravitationally unstable and collapse into dense cores, and eventually turn into new stars (Elmegreen & Scalo 2004; Mac Low & Klessen 2004; McKee & Ostriker 2007). Statistical quantities describing this process, such as the initial mass function (IMF), the core mass function (CMF; Padoan & Nordlund 2002; Hennebelle & Chabrier 2008, 2009), and the star formation rate (Hennebelle & Chabrier 2011; Padoan & Nordlund 2011) depend on the standard deviation (std. dev.) of the density of the molecular cloud. The pioneering works of Padoan et al. (1997) and Passot & Vázquez-Semadeni (1998) have shown that the std. dev. σ_ρ of the probability density function (PDF) of the mass density grows proportionally to the root-mean-square (rms) Mach number $\mathcal{M}$ of the turbulent flow,

$$\sigma_\rho / \langle \rho \rangle_V = b\,\mathcal{M}, \tag{1}$$

where $\langle \rho \rangle_V$ is the volume-weighted mean density and b is a proportionality constant. A solid understanding of the interplay between the highly turbulent velocity field and the resulting statistical properties of the density distribution is not just important for models of star formation theory, but also for other fields of astrophysics, such as the diffuse interstellar medium (e.g., Hill et al. 2008; Burkhart et al. 2010; Gaensler et al. 2011), galaxy evolution (e.g., Bigiel et al. 2008), or galactic and protogalactic dynamos (e.g., Beck 1996; Schober et al. 2012). Federrath et al. (2008, 2010) explained the dependence of σ_ρ

on b by taking into account the modes of the forcing that drive the turbulent velocity field. This model predicts $b = 1/3$, for purely solenoidal forcing, and $b = 1$ for purely compressive forcing, and explains the large deviations of b ranging from $b = 0.26$ to $b = 1.05$ in previous works (e.g., Padoan et al. 1997; Passot & Vázquez-Semadeni 1998; Li et al. 2003; Kritsuk et al. 2007; Beetz et al. 2008; Schmidt et al. 2009; Price et al. 2011; Burkhart & Lazarian 2012; Konstandin et al. 2012; Molina et al. 2012). We follow up on this work and discuss the physical origin of this dependence, and introduce a new relation, similar to Equation (1), correlating the compressible component of the rms Mach number $\mathcal{M}_{\mathrm{comp}}$ with σ_ρ.

In Section 2 we explain our numerical setup. We analyze the influence of measuring mass-weighted and volume-weighted distributions in Section 3.1, the influence of the resolution on our measurements in Section 3.2, and the PDFs of the mass density and the compressible part of the velocity field in Section 3.3. In Section 3.4 we present the linear relations between the std. dev. of the mass density and the rms Mach number. In Section 3.5 we discuss the new relation between the std. dev. of the mass density and that of the compressible part of the velocity field. A summary of our results and conclusions is given in Section 4.

2. SIMULATIONS AND METHODS

We use the piecewise parabolic method (Colella & Woodward 1984) implemented in the grid code FLASH3 (Fryxell et al. 2000; Dubey et al. 2008) to solve the hydrodynamical equations on a uniform three-dimensional grid. These equations are the continuity equation

$$\frac{\partial \rho}{\partial t} + (\mathbf{v} \cdot \nabla)\rho = -\rho \nabla \cdot \mathbf{v}, \tag{2}$$
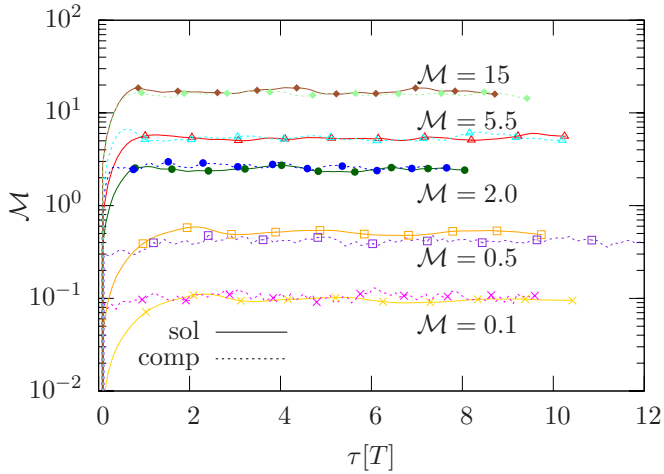
Figure 1. rms Mach number of all simulations as a function of the dynamical timescale, calculated by averaging over all grid cells for both types of forcing.
(A color version of this figure is available in the online journal.)

the Euler equation with a stochastic forcing term $\mathbf{F}$ per unit mass

$$\frac{\partial \mathbf{v}}{\partial t} + (\mathbf{v} \cdot \nabla)\mathbf{v} = -\frac{\nabla p}{\rho} + \mathbf{F}, \qquad (3)$$

and the equation of state

$$p = \kappa \rho^{\Gamma}, \qquad (4)$$

where $\mathbf{v}$ is the velocity field, $s = \ln(\rho/\langle\rho\rangle_V)$ is the natural logarithm of the mass density ρ, c_s is the sound speed, p is the pressure, and Γ is the adiabatic index. Since isothermal gas is assumed throughout this study, $\Gamma = 1$, the pressure, $p = \rho c_s^2$, is proportional to the mass density with a fixed sound speed c_s. These simulations are scale free, so we set $\langle\rho\rangle_V = 1$, $c_s = 1$, and the box size of the simulation $L = 1$. The numerical simulations are set to evolve for 10 dynamical timescales $T = L/(2\mathcal{M}c_s)$, where $\mathcal{M} = v_{\mathrm{r.m.s.}}/c_s$ is the rms Mach number of the simulations with the rms velocity $v_{\mathrm{r.m.s.}}$. All relevant quantities are stored in intervals of $0.1T$. The stochastic forcing field $\mathbf{F}$ has an autocorrelation time equal to the dynamical timescale on the injection scale, which depends on the resulting rms Mach number of the simulation in the state of statistically stationary, fully developed turbulence. The forcing field is constructed in Fourier space such that the kinetic energy is injected on the largest scales, where $1 < kL/2\pi < 3$ and it varies smoothly in space and time. To analyze the influence of different modes of the forcing field, we use projection tensors in Fourier space to get a purely divergence-free, $\nabla \cdot \mathbf{F} = 0$, solenoidal or a purely curl-free, $\nabla \times \mathbf{F} = 0$, compressive vector field for the forcing. We adjust the amplitude of the forcing such that we have $\mathcal{M} = 0.1, 0.5, 2, 5.5, 15$ for both types of forcing in the stationary state of fully developed turbulence. To investigate the effects of numerical viscosity, we study simulations at different resolutions: $128^3, 256^3, 512^3$, and 1024^3. The parameters of these simulations are described in Konstandin et al. (2012), and a detailed description of the forcing is presented in Schmidt et al. (2009) and Federrath et al. (2010).

3. RESULTS

Figure 1 shows the time evolution of $\mathcal{M}$ in all simulations. The fluid reaches the equilibrium state of fully developed turbulence after about two turbulent crossing times $t \approx 2T$. We thus average all the following analyses for $2 \leqslant t/T$.
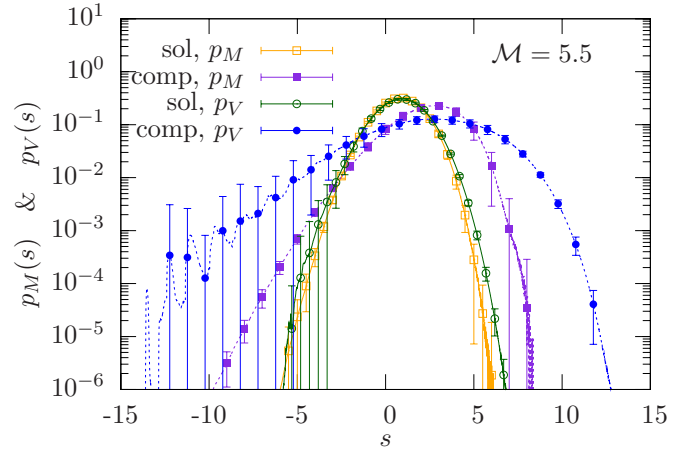

Figure 2. Mass-weighted and volume-weighted PDFs of the logarithm of the mass density in the simulations with $\mathcal{M} = 5.5$, 1024^3 grid cells and both types of forcing.
(A color version of this figure is available in the online journal.)

3.1. Volume-weighted and Mass-weighted Probability Density Functions

It is well known that the PDF of the logarithm of the mass density $p(s)$ in a turbulent, isothermal medium is close to a Gaussian distribution (see, e.g., Vazquez-Semadeni 1994; Passot et al. 1994; Padoan et al. 1997; Klessen 2000; Kritsuk et al. 2007; Federrath et al. 2008; Konstandin et al. 2012):

$$p(s) = \frac{1}{\sqrt{2\pi}\sigma_s} \exp\left(\frac{-(s - \langle s\rangle)^2}{2\sigma_s^2}\right). \qquad (5)$$

Li et al. (2003) showed with the assumption of a Gaussian, volume-weighted PDF of s that the mass-weighted PDF of s is also Gaussian with the same std. dev. and with a shifted mean value,

$$\langle s\rangle_V = -\langle s\rangle_M = -\frac{\sigma_s^2}{2}. \qquad (6)$$

Figure 2 shows the volume- and mass-weighted PDFs (the volume-weighted PDF is shifted by $\langle s\rangle_M - \langle s\rangle_V = \sigma_s^2$ for better comparison) for the simulation with $\mathcal{M} = 5.5$ for both types of forcing. The PDFs are averaged over 81 time snapshots in the state of fully developed stationary turbulence for $t \geqslant 2T$ and the error bars indicate the std. dev. of the temporal fluctuations. The variance of the volume-weighted PDFs is larger than that of the mass-weighted distributions. This effect is stronger for the compressive than for the solenoidal forcing. The volume-weighted PDFs show a larger variation with time in the low-density wing of the distribution than the mass-weighted distributions. This low-density wing also shows higher probabilities than one would expect from the underlying Gaussian distribution extrapolated from the high-density wing. This effect is stronger for the compressive than for the solenoidal forcing. We assume that this behavior is caused by our forcing scheme. As the time correlation of the forcing field is equal to the dynamic timescale on the largest scales, the forcing has enough time to produce very low densities in large regions of diverging flows. This process causes the volume-weighted PDF of s to have a tail at low densities with higher probabilities than the distribution for the case of turbulence, which is not driven on the largest scales. As this effect is proportional to the amplitude of the forcing field, which increases more strongly than $\mathcal{M}$ in
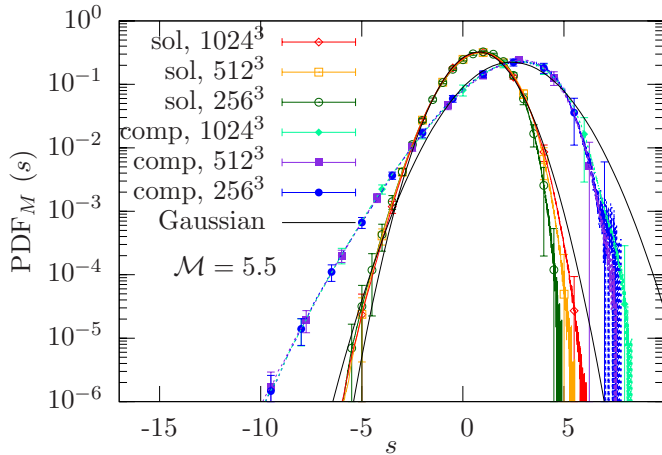
Figure 3. Mass-weighted PDFs of s of the simulations for $\mathcal{M} = 5.5$, different resolutions, and both types of forcing. The black solid lines are Gaussian functions with mean value and std. dev. calculated with the highest resolution.

(A color version of this figure is available in the online journal.)

the statistically stationary state of fully developed turbulence, it becomes more important for higher $\mathcal{M}$ and the deviations in the low-density tail influence the calculated std. dev. of these distributions. This effect is less pronounced when measuring the mass-weighted distributions, as the very low density grid cells carry only little mass. We note that there are other potential processes that could lead to non-Gaussian wings in the PDF, such as turbulent intermittency or self-gravity (e.g., Klessen 2000; Kritsuk et al. 2007; Burkhart et al. 2009; Federrath et al. 2010).

3.2. Resolution Effects on the Probability Density Functions

Figure 3 shows the mass-weighted PDF of the quantity s with $\mathcal{M} = 5.5$ and different resolutions. The PDF of s shows deviations from the Gaussian shape and a dependence on the resolution only in the high-density tails of the distribution. We interpret the deviations of our measured PDFs from the Gaussian distribution in the supersonic regime for both types of forcing as a sign of numerical dissipation and finite sampling.

In the highly supersonic regime the medium is dominated by shock fronts, high-density gradients, and strong intermittent fluctuations, which are building up in the high-density tail and require high resolution to converge. As the high-density tail is always truncated due to limited numerical resolution (see Hennebelle & Audit 2007; Kowal et al. 2007; Kitsionas et al. 2009; Price & Federrath 2010; Federrath et al. 2010), we do not fully resolve them in the $\mathcal{M} = 5.5$ case and an additional dissipation occurs. This effect is stronger in the simulations with compressive forcing and becomes stronger with increasing $\mathcal{M}$ for both types of forcing (not shown here). However, increasing the resolution has only little influence on the deviations from the Gaussian distribution in the low-density tail of the mass-weighted PDFs.

With the assumption of a log–normally distributed mass density, it can be shown that the std. dev. of the Gaussian-distributed quantity s is (see Price et al. 2011)

$$\sigma_s^2 = \ln\left(1 + \sigma_\rho^2\right). \tag{7}$$

Figure 4 shows σ_ρ as a function of σ_s for our volume-weighted (left panel) and mass-weighted (right panel) distributions. The volume- and mass-weighted measurements of the std. dev. of s show increasing deviations from Equation (7) with increasing $\mathcal{M}$ for both types of forcing. However, the deviations are smaller in the mass-weighted case than in the volume-weighted one. The assumption of Gaussianity, which is implied in Equation (7), is better fulfilled for the mass-weighted case. Figure 4 also shows that our measurements with $\mathcal{M} = 15$ do not converge with resolution for both types of forcing. They are in agreement with those of Price et al. (2011), who showed that direct measurements of σ_ρ show a stronger dependence on resolution than measurements of σ_s.

All volume-weighted measurements show a clear trend toward relation (7) with increasing resolution. However, the data points do not fit relation (7) for $\mathcal{M} = 15$ with solenoidal forcing and in all the supersonic cases with compressive forcing, although the data points with $\mathcal{M} = 2$ and $\mathcal{M} = 5.5$ with compressive forcing nearly converge with resolution. Considering that the std. dev. $\sigma_{s,M}$ of the mass-weighted PDF is more compatible with the scaling for a log–normal PDF, Equation (7), and that the resolution dependence of $\sigma_{s,M}$ is weaker than for $\sigma_{s,V}$,
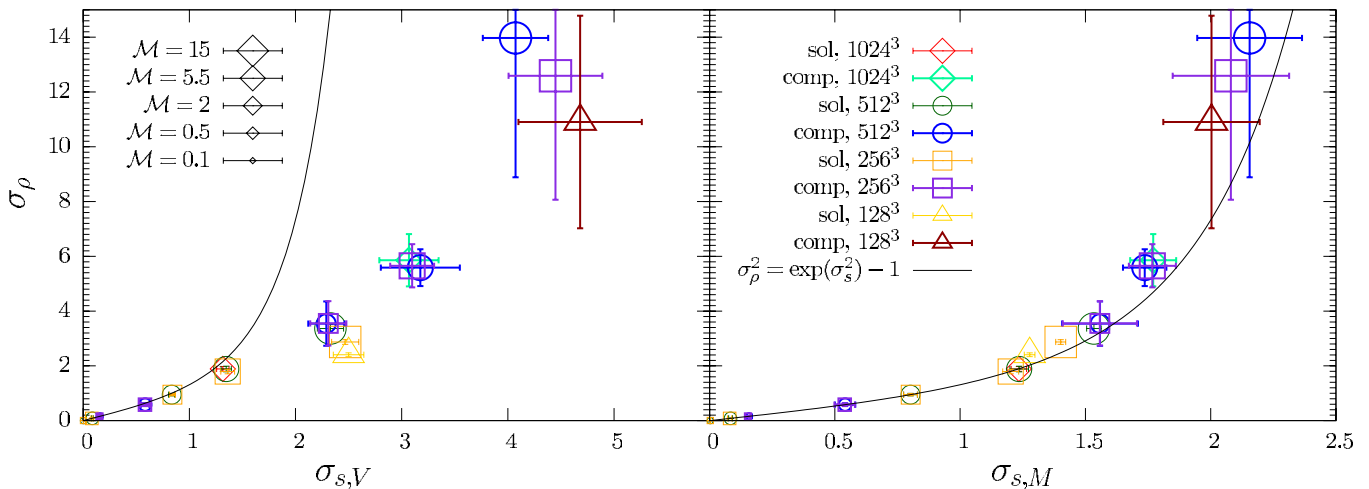

Figure 4. Std. dev. of the mass density σ_ρ as a function of the std. dev. of the logarithm of the mass density σ_s, measured volume-weighted (left panel) and mass-weighted (right panel). The deviations of the measurements from the black solid lines, Equation (7), quantify the deviations from a log–normally distributed mass density.

(A color version of this figure is available in the online journal.)

we prefer to use $\sigma_{s,M}$ as an estimate for the turbulent density fluctuations in the following.

3.3. The Probability Density Function of the Density and of the Compressible Modes in the Velocity Field

Figure 5 shows the mass-weighted PDFs of the quantity s (left panels) and the volume-weighted PDFs of the compressible modes of the velocity field normalized to the sound speed $M_{\rm comp} = v_{\rm comp}/c_s$ (right panels) for different $\mathcal{M}$ and both types of forcing. The PDFs of the logarithm of the density largely follow Gaussian distributions for all supersonic $\mathcal{M}$. We added Gaussian functions (black solid lines) with the first- and second-order moments calculated from our distributions in Figure 5. The high-density tails of the distributions show deviations from the Gaussian shape, which increase with increasing $\mathcal{M}$. Also, the deviations from the Gaussian distribution in the low-density tail, as discussed in Section 3.1, become more pronounced with increasing $\mathcal{M}$. Thereby, we have large deviations of our measurement from the Gaussian distributions in the $\mathcal{M} = 15$ case and the calculated std. dev. does not correspond to that of the underlying Gaussian distribution.

The density distributions of the simulations driven by solenoidal forcing in the subsonic regime show significant deviations from the log–normal shape, which become stronger as $\mathcal{M}$ decreases. These distributions become more asymmetric and more peaked. The different behavior of the PDFs in the subsonic regime, especially for the solenoidal forcing, is caused by the different physical processes acting here. In the subsonic regime sound waves transfer information faster than the averaged flow of the medium, such that the thermal pressure increases before two converging flows can collide. This process prevents colliding flows from producing high-density regions and causes the sharp edge at the high-density wing of the distributions. The thermal pressure also decelerates the velocities in compressible modes, such that the PDF of $M_{\rm comp}$ also shows a narrow, peaky, and intermittent behavior for the solenoidal forcing. This process is just visible for solenoidal forcing, because in the compressive forcing case the velocities in compressible modes are re-injected by the forcing to hold $\mathcal{M}$ constant. This is why the thermal pressure does not have such a strong influence there.

The right panels of Figure 5 show the PDFs of $M_{\rm comp}$, where $M_{\rm comp}$ is calculated by transforming the velocity field into Fourier space and applying the same projection tensor we use for the forcing field, $P_{ij}^{\parallel} = k_i k_j / k^2$. After transforming it back into real space, we calculate the std. dev. of the components, which we average afterwards over the three directions of the coordinate system, x, y, z. The distributions of $M_{\rm comp}$ are symmetric with zero mean and have an increasing std. dev. with increasing $\mathcal{M}$. The distributions obtained with compressive forcing are always broader than with solenoidal forcing at the same value of $\mathcal{M}$. The PDFs of $M_{\rm comp}$ are Gaussian (black solid lines) with deviations in both wings. These are the signposts of turbulent intermittency. The deviations do not show a clear trend with the $\mathcal{M}$.

The PDF of $M_{\rm comp}$ obtained with solenoidal forcing in the subsonic regime with $\mathcal{M} = 0.1$ shows the strongest deviations from the Gaussian shape with a narrow, peaky, intermittent distribution. These deviations are caused by the thermal pressure, as discussed above.

3.4. Relation between $\mathcal{M}$ and the Standard Deviation of the Density

In Padoan et al. (1997) and Passot & Vázquez-Semadeni (1998) the authors found that the std. dev. of the PDF of the

mass density σ_ρ is proportional to $\mathcal{M}$ in a turbulent flow. The std. dev. of the mass density is an important quantity, especially in astrophysics, where the Mach number dependence of density fluctuations is used to derive analytic expressions for the CMF and the stellar IMF (e.g., Padoan & Nordlund 2002; Hennebelle & Chabrier 2008, 2009). On galactic scales it is used to reproduce the Kennicutt–Schmidt relation (Tassis 2007), and Elmegreen (2008) suggests that the star formation efficiency is a function of the density PDF. Figure 6 (upper left panel) shows the measured std. dev. of the mass density as a function of $\mathcal{M}$ for different resolutions and both types of forcing. The error bars in each panel of Figure 6 indicate the std. dev. of the temporal fluctuations of the measured quantities. They do not include any potential systematic errors stemming from, e.g., the numerical scheme or implementation of the forcing algorithm. Thus, we interpret the error bars as a lower limit of the real uncertainty. The dotted and dashed-dotted lines correspond to the model of Federrath et al. (2010), which describes the proportionality parameter b as a function of the turbulent forcing. This model predicts $b = 1/3$ for solenoidal forcing and $b = 1$ for compressive forcing. Our measurements agree with the model of Federrath et al. (2010) in the supersonic case for both types of forcing. We see small deviations from the model in the simulations with $\mathcal{M} = 15$, which are caused by our limited resolution (see Figure 4). The std. dev.s of the density distribution of the simulation with solenoidal forcing are smaller than the prediction of the model in the subsonic case. In the subsonic regime, the deviations are caused by the thermal pressure, which damps density variations and compressible modes of the velocity field and reduces the measured std. dev. below the model prediction as discussed in Section 3.3. The upper right panel of Figure 6 shows the mass-weighted, logarithmic std. dev. $\sigma_{s,M}$ as a function of $\mathcal{M}$. The dotted and dashed-dotted lines correspond to the standard model for the logarithmic density variance,

$$\sigma_s^2 = \ln(1 + b^2 \mathcal{M}^2), \qquad (8)$$

with $b = 1/3$ for solenoidal and $b = 1$ for compressive forcing. Equation (8) follows from Equations (1) and (7) and was recently derived analytically by Molina et al. (2012) using the shock-jump conditions and averaging over an ensemble of shock waves. The deviations of our numerical data from this standard model are only significant for solenoidal forcing in the subsonic regime, while our data are in excellent agreement with Equation (8) for both solenoidal and compressive forcing in the supersonic regime, given our resolution dependence of the $\mathcal{M} = 15$ data points (see Figure 4, right panel). Our results are in agreement with those of Kowal et al. (2007), who found deviations from the linear relation with σ_ρ in the subsonic regime with solenoidal forcing, and with Passot & Vázquez-Semadeni (1998), who analyzed one-dimensional simulations with only compressive forcing and $0.5 \leqslant \mathcal{M} \leqslant 3$ and found a linear relation between $\mathcal{M}$ and σ_ρ with $b = 1$. Price et al. (2011) analyzed three-dimensional simulations with purely solenoidal forcing and values of $\mathcal{M}$ between $2 \leqslant \mathcal{M} \leqslant 20$ and found $b = 1/3$, in excellent agreement with our result. As they did not analyze the subsonic regime with solenoidal forcing they did not observe the large deviations in the subsonic regime. Our analysis complements these studies with measurements in both the subsonic and supersonic regimes and for purely compressive forcing.
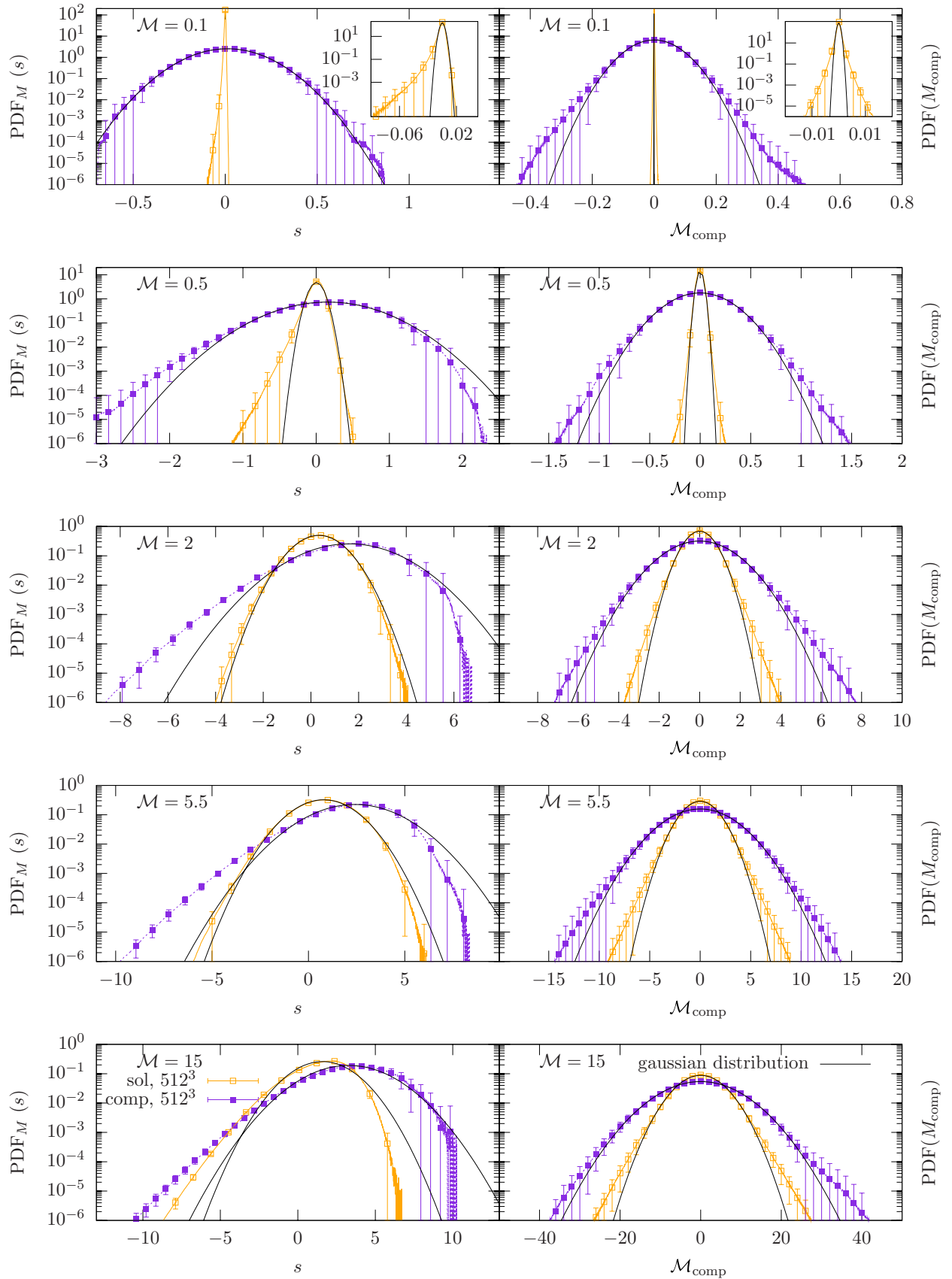
Figure 5. Mass-weighted PDFs of the logarithm of the mass density (left panels) and the compressible part of the local Mach number (right panels) for different $\mathcal{M}$, resolutions, and both types of forcing. In the inset, a magnification of the PDFs obtained with solenoidal forcing for $\mathcal{M} = 0.1$ is shown. The error bars in each panel indicate the std. dev. of the temporal fluctuations.
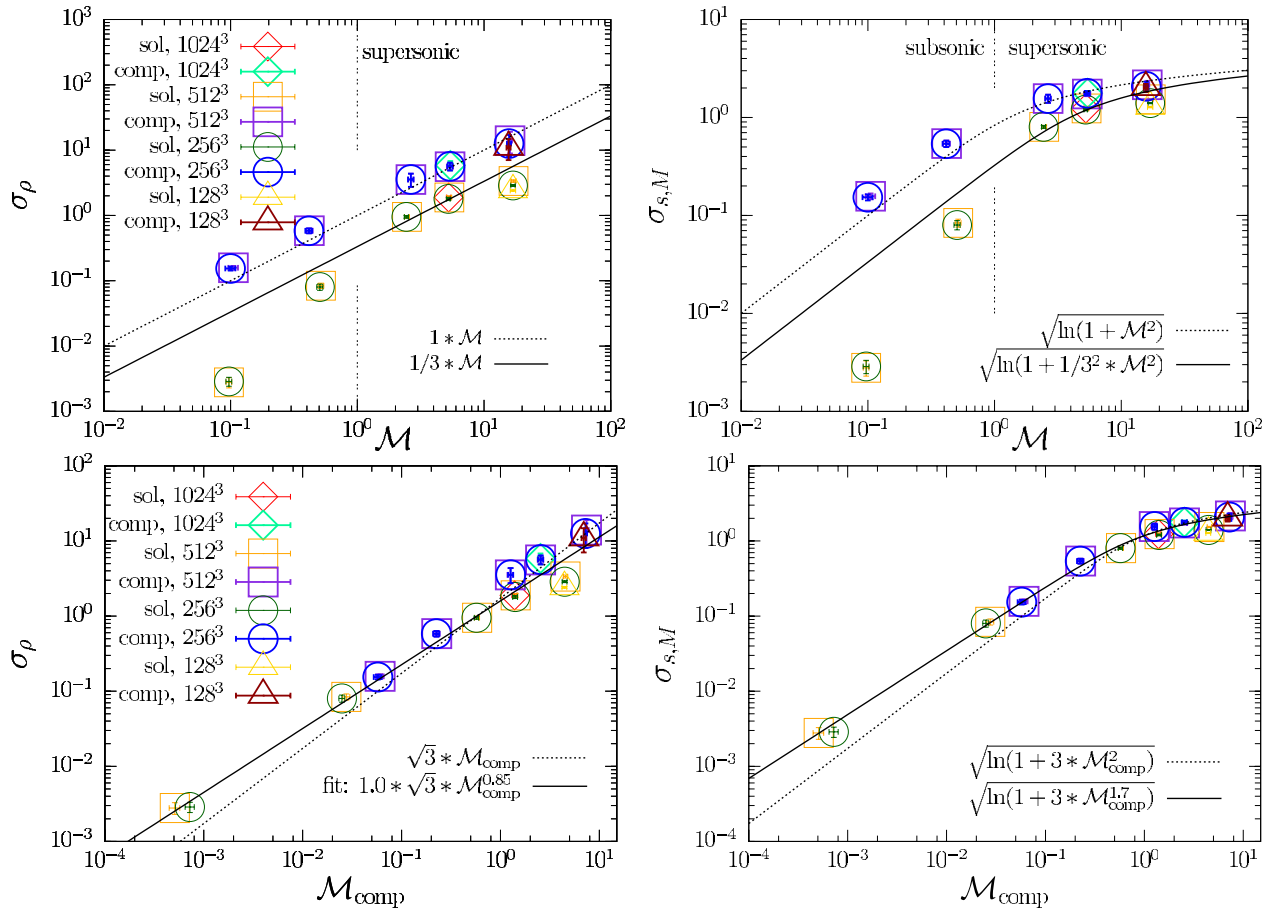
(A color version of this figure is available in the online journal.)

Figure 6. Std. dev. of the distribution of the mass density (left) and std. dev. of the distribution of the logarithm of the mass density (right) as a function of $\mathcal{M}$ (upper panels) and as a function of $\mathcal{M}_{\mathrm{comp}}$ (lower panels). In the upper panels, the lines correspond to the model of Federrath et al. (2010) with $b = 1/3$ for solenoidal forcing and $b = 1$ for compressive forcing. In the lower panels, the solid lines correspond to a two-parameter fit and the dotted line corresponds to a linear relation between the std. dev. of the mass density and that of $\mathcal{M}_{\mathrm{comp}}$ with a proportionality constant $\sqrt{3}$.

(A color version of this figure is available in the online journal.)

3.5. Physical Origin of Density Fluctuations in Turbulent Flows

Looking at the continuity Equation (2), one can argue that variations of the density can only be caused by the divergence of the velocity field. Given that a vector field can be decomposed in a gradient field and a rotation field, and that the divergence of the rotation field vanishes, we conclude that the density variations can only be caused by the compressible modes of the velocity. A similar model has also been suggested by Federrath et al. (2010), where the parameter b in Equations (1) and (8) was approximated by the ratio of compressible to total velocity fluctuations. As we want to understand the physical origin of the density fluctuations, we replace $\mathcal{M}$ and the b-parameter with $\mathcal{M}_{\mathrm{comp}}$, in Equation (1), where $\mathcal{M}$ is in fact the std. dev. of the velocity distribution, and b is proportional to the ratio of compressible to total velocity fluctuations and depends on the forcing. The lower panels of Figure 6 show the density fluctuations as a function of $\mathcal{M}_{\mathrm{comp}}$. The data points show a clear correlation. The different behavior of the simulations driven with solenoidal and compressive forcing is significantly reduced. In Figure 6 we added a function (dotted line) for the relation $\sigma_\rho = \sqrt{3}\mathcal{M}_{\mathrm{comp}}$, which is the simplest model for this relation assuming isotropy. The factor of $\sqrt{3}$ is due to the fact that we use the distribution of the compressible modes of the velocity field averaged over the three directions of the

coordinate system,

$$\mathcal{M}^{\mathrm{tot}}_{\mathrm{comp}} = \sqrt{\mathcal{M}^2_{\mathrm{comp},\,x} + \mathcal{M}^2_{\mathrm{comp},\,y} + \mathcal{M}^2_{\mathrm{comp},\,z}}$$
$$= \sqrt{3}\mathcal{M}_{\mathrm{comp}}. \quad (9)$$

Our simple model fits the data, but shows deviations for the simulations with solenoidal forcing and the lowest and highest Mach numbers. The deviations for the $\mathcal{M} = 15$ simulation are again caused by the resolution dependence of σ_ρ. Additionally, we perform a fit of our data (black solid line) with two free parameters,

$$\sigma_\rho = \alpha\sqrt{3}\mathcal{M}^\beta_{\mathrm{comp}}, \quad (10)$$

for the density relation. We obtain a normalization $\alpha = 1.0 \pm 0.1$ and a slope $\beta = 0.85 \pm 0.04$. For the s-relation we transform the fitted function with Equation (7). The measurements of the std. dev. of the density have larger deviations from the model than those of the std. dev. of s. However, the model fits the measurements in both cases and provides a good description for the data points in the subsonic regime with solenoidal forcing, which are strongly influenced by sound waves. We conclude that the thermal pressure damps the velocities in compressible modes in such a way that the relation between the velocities in compressible modes and the density variations in a turbulent medium is in a statistical equilibrium state, even if the medium is strongly influenced by sound waves. The deviation of the

scaling exponent from the simple model can be interpreted as additional dissipative effects, which are proportional to $\mathcal{M}_{\mathrm{comp}}$. An example of these physical processes which influence our analysis are individual shocks causing deviations from the log–normal-distributed density PDF. However, systematic errors with a dependence on $\mathcal{M}$ could also cause deviations from the linear scaling and would be another possible interpretation for our fitted scaling exponent.

The relation between the std. dev. of the density and the compressible part of $\mathcal{M}$ in principle enables us to measure the kinetic energy in compressible modes in giant molecular clouds, without knowing the absolute $\mathcal{M}$, the driving mechanism, or the sound speed. The relations shown in the bottom panels of Figure 6 are valid in both the subsonic and supersonic regime.

4. SUMMARY AND CONCLUSIONS

We have investigated the influence of solenoidal (divergence-free) and compressive (curl-free) forcing on the PDF of the mass density in subsonic and supersonic turbulence with a set of three-dimensional numerical simulations. We analyzed the relation between the std. dev. of the mass density distribution and the rms Mach number, $\mathcal{M}$. We found a new relation between the std. dev. of the mass density and that of the compressible part of the velocity field, $\sigma_\rho \propto \mathcal{M}_{\mathrm{comp}}$. Our main results are as follows.

1. Compressive forcing yields mass density PDFs with std. dev. proportional to $\mathcal{M}$ with $b = 1$. For solenoidal forcing, we measure $b = 1/3$ in the supersonic regime. Our findings are in agreement with previous studies which, however, only explored different subsets of the full parameter space investigated here. We also found deviations of our measurements from the linear relation with solenoidal forcing in the subsonic regime. These deviations from the linear relation can be explained as resulting from sound waves, which damp the faint compressible velocities and prevent the medium from producing overdensities.

2. We found a unique relation between the std. dev. of the mass density and the compressible modes of the velocity field with a fit to our data. Our new relation is independent of the driving mechanism and still holds in the subsonic regime, where the flow is mainly influenced by sound waves. It does not show a strong influence on the resolution and other effects, which may cause a non-Gaussian distribution of the density.

3. Our relation enables us for the first time to measure the kinetic energy in compressible modes in units of the sound speed, without knowing $\mathcal{M}$, the driving mechanism, or the sound speed of the medium. This measurement can be used to distinguish between subsonic and supersonic compressive turbulent motions. It will in principle allow us to measure the composition of the kinetic energy in the interstellar medium by combining independent measurements of the total $\mathcal{M}$ (e.g., Burkhart et al. 2009) and the std. dev. of the density distribution (Brunt et al. 2010; Brunt 2010; Schneider et al. 2012).

REFERENCES

Beck, R. 1996, Nachr. Akad. Wiss. Göttingen II, Jahrg., 4, 262
Beetz, A., Gollwitzer, C., Richter, R., & Rehberg, I. 2008, J. Phys. Condens. Matter, 20, 204109
Bigiel, F., Leroy, A., Walter, F., et al. 2008, AJ, 136, 2846
Brunt, C. M. 2010, A&A, 513, A67
Brunt, C. M., Federrath, C., & Price, D. J. 2010, MNRAS, 403, 1507
Burkhart, B., Falceta-Gonçalves, D., Kowal, G., & Lazarian, A. 2009, ApJ, 693, 250
Burkhart, B., & Lazarian, A. 2012, ApJ, 755, L19
Burkhart, B., Stanimirović, S., Lazarian, A., & Kowal, G. 2010, ApJ, 708, 1204
Colella, P., & Woodward, P. R. 1984, J. Comput. Phys., 54, 174
Dubey, A., Fisher, R., Graziani, C., et al. 2008, in ASP Conf. Ser. 385, Numerical Modeling of Space Plasma Flows, ed. N. V. Pogorelov, E. Audit, & G. P. Zank (San Francisco, CA: ASP), 145
Elmegreen, B. G. 2008, ApJ, 672, 1006
Elmegreen, B. G., & Scalo, J. 2004, ARA&A, 42, 211
Federrath, C., Klessen, R. S., & Schmidt, W. 2008, ApJ, 688, L79
Federrath, C., Roman-Duval, J., Klessen, R. S., Schmidt, W., & Mac Low, M. 2010, A&A, 512, A81
Fryxell, B., Olson, K., Ricker, P., et al. 2000, ApJS, 131, 273
Gaensler, B. M., Haverkorn, M., Burkhart, B., et al. 2011, Nature, 478, 214
Hennebelle, P., & Audit, E. 2007, A&A, 465, 431
Hennebelle, P., & Chabrier, G. 2008, ApJ, 684, 395
Hennebelle, P., & Chabrier, G. 2009, ApJ, 702, 1428
Hennebelle, P., & Chabrier, G. 2011, ApJ, 743, L29
Hill, A. S., Benjamin, R. A., Kowal, G., et al. 2008, ApJ, 686, 363
Kitsionas, S., Federrath, C., Klessen, R. S., et al. 2009, A&A, 508, 541
Klessen, R. S. 2000, ApJ, 535, 869
Konstandin, L., Federrath, C., Klessen, R. S., & Schmidt, W. 2012, J. Fluid Mech., 692, 183
Kowal, G., Lazarian, A., & Beresnyak, A. 2007, ApJ, 658, 423
Kritsuk, A. G., Norman, M. L., Padoan, P., & Wagner, R. 2007, ApJ, 665, 416
Li, Y., Klessen, R. S., & Mac Low, M. 2003, ApJ, 592, 975
Mac Low, M.-M., & Klessen, R. S. 2004, Rev. Mod. Phys., 76, 125
McKee, C. F., & Ostriker, E. C. 2007, ARA&A, 45, 565
Molina, F. Z., Glover, S. C. O., Federrath, C., & Klessen, R. S. 2012, MNRAS, 423, 2680
Padoan, P., & Nordlund, Å. 2002, ApJ, 576, 870
Padoan, P., & Nordlund, Å. 2011, ApJ, 730, 40
Padoan, P., Nordlund, A., & Jones, B. J. T. 1997, MNRAS, 288, 145
Passot, T., & Vázquez-Semadeni, E. 1998, Phys. Rev. E, 58, 4501
Passot, T., Vázquez-Semadeni, E. C., & Pouquet, A. 1994, in Numerical Simulations in Astrophysics: Modelling the Dynamics of the Universe, ed. J. Franco, S. Lizano, L. Aguilar, & E. Daltabuit (Cambridge: Cambridge Univ. Press), 246
Price, D. J., & Federrath, C. 2010, MNRAS, 406, 1659
Price, D. J., Federrath, C., & Brunt, C. M. 2011, ApJ, 727, L21
Schmidt, W., Federrath, C., Hupp, M., Kern, S., & Niemeyer, J. C. 2009, A&A, 494, 127
Schneider, N., Csengeri, T., Hennemann, M., et al. 2012, A&A, 540, L11
Schober, J., Schleicher, D., Federrath, C., Klessen, R., & Banerjee, R. 2012, Phys. Rev. E, 85, 026303
Tassis, K. 2007, MNRAS, 382, 1317
Vazquez-Semadeni, E. 1994, ApJ, 423, 681